Supplementary data for

Thiadiazolophenanthroline-Based Hole-Transporter for Durable and Efficient Perovskite Solar Cells: Atomic-Level Insights on Performance Increase

Zhu-Zhu Sun,*[,a] Yang Li,[a] Yunhai Zhang,[a] Quan-Song Li[b] and Wei-Lu Ding*[,c]

[a]*College of Physics and Electronic Engineering, Heze University, Heze 274015, China*

[b]*Beijing Key Laboratory of Photoelectronic/Electrophotonic Conversion Materials, Key Laboratory of Cluster Science of the Ministry of Education, School of Chemistry and Chemical Engineering, Beijing Institute of Technology, Beijing 100081, China*

[c]*Beijing Key Laboratory of Ionic Liquids Clean Process, CAS Key Laboratory of Green Process and Engineering, State Key Laboratory of Multiphase Complex Systems, Institute of Process Engineering, Chinese Academy of Sciences, Beijing 100190, China*

E-mail: Z.Z.Sun: sunzhuzhu@hezeu.edu.cn; W.L.Ding: wlding@ipe.ac.cn

Contents

Computational approaches

1 Theoretical framework

Due to the limited charge transfer interaction in organic conductive materials, the Marcus hopping model in conjunction with the Einstein equation is typically used to analyze the charge transport characteristics of HTMs.[1,2] Therefore, we employed this method in our work. Based on the Marcus theory, the charge hopping rate κ is given by the following expression:[3]

$$\kappa = \frac{2\pi}{\hbar} V_{ab}^{2} \frac{1}{\sqrt{4\pi\lambda k_B T}} exp\left[-\lambda / 4k_B T \right]$$

where V_{ab}, λ, $\hbar$, k_B and T show transfer integral, reorganization energy, Planck's constant, Boltzmann's constant and temperature (in Kelvin), respectively.

Herein, the reorganization energy was assessed by the adiabatic potential energy surface method,[4,5] while the transfer integral was evaluated through a direct coupling approach according to the simulated hole hopping pathways[6,7]

$$V_{ab} = \left\langle \psi_{HOMO}^{0,a} \middle| F \middle| \psi_{HOMO}^{0,b} \right\rangle$$

where $\psi_{HOMO}^{0,a}$ and $\psi_{HOMO}^{0,b}$ are the HOMOs of adjacent molecules *a* and *b* without intermolecular interactions, and F is the Fock operator for dimers.

Hence, the hole mobility (μ) of the studied system can be derived based on the Einstein relationship[8]

$$\mu = \frac{eD}{k_B T}$$

where e is the unit charge, and D is the diffusion coefficient, with formula as

$$D = \frac{1}{2d} \sum_{i} r_i^2 k_i p_i$$

where i is the hole transfer pathway, r_i is the centroid to centroid distance, d is the spatial dimensionality and presumed to be 1 in this paper,[9] and p_i ($p_i = k_i \Big/ \sum_i k_i$) is the relative probability for hole hopping to the *i*-th pathway.

2 Calculational procedures

Optimization of the ground- and excited-state molecular geometries was carried out using the B3LYP/6-31G** and CAM-B3LYP/6-31G** methods, respectively.[10,11] On the basis of optimized ground-state geometries, the light absorption spectra were simulated by the MPW1K/6-31G** and CAM-B3LYP/6-31G** approaches.[12,13] The dichloromethane (DCM) solvent effect was simulated with the C-PCM method,[14] and vibrational calculation was confirmed energetic minima with no imaginary frequency detected. The transferred charge amounts and distances, and CDD maps by employing the methodology outlined by Ciofini et al.[15] The CDD map was executed by utilizing the Multiwfn 3.3.8 software,[16] leveraging Gaussian outputs as the basis. Particularly, the SMD model, coupled with the M05-2X/6-31G** method are used to simulate the solvation Gibbs free energies.[17] All computations were conducted using the Gaussian 09 software.[18]

To obtain the stable dimers for hole transfer, the 30 ps molecular dynamics (MD) simulations were carried out firstly with the DFTB+ 1.2.2 package.[19] The 3ob-3-1 SK parameters for C, N, O, S and H, and the NVE ensemble were employed. Based on the rough dimers, which come from dynamic simulations with the lowest energies, the energy optimizations were further implemented with the Gaussian 09 package at the B3LYP/6-31G** level to get accurate dimeric geometries. The dispersion corrections

were also considered with B3LYP-D3 model. Finally, the hole transfer integrals were achieved by the PW91PW91/6-31G** method,[20,21] which has been shown as a better choice for describing of intermolecular hole coupling at the DFT level.

The PbI_2-terminated (100) surfaces of cubic $FAPbI_3$ are employed to research the adsorbed influences of HTMs.[22] The surfaces are composed of (3×5) supercells, and a vacuum of 25 Å is added in z direction to avoid periodic interactions. All calculations are performed by the Vienna ab initio package (VASP).[23-24] The GGA-PBE functional and the projector-augmented wave pseudopotential are used to describe the exchange and correlation interactions.[25-26] The spin polarization and an energy cutoff of 400 eV are utilized to achieve the energy and force convergence of 0.1 meV and 20 meV $Å^{-1}$, respectively. Meanwhile, the Grimme's D3 method is also considered to describe the weak van der Waals interactions.[27]

References

1. L. J. Wang, G. J. Nan, X. D. Yang, Q. Peng, Q. K. Li and Z. G. Shuai, *Chem. Soc. Rev.*, 2010, **39**, 423-434.
2. Y. A. Duan, H. B. Li, Y. Geng, Y. Wu, G. Y. Wang and Z. M. Su, *Org. Electron.*, 2014, **15**, 602-613.
3. R. A. Marcus and N. Sutin, *Biochim. Biophys. Acta*, 1985, **811**, 265-322.
4. Z. Z. Sun, S. Feng and W. L. Ding, *Synth. Met.*, 2020, **259**, 116219.
5. Z. Z. Sun, S. Feng, W. L. Ding, J. Yang, X. R. Zhu, J. L. Liu and X. L. Xu, *Synth. Met.*, 2022, **289**, 117136.
6. G. J. Nan, L. J. Wang, X. D. Yang, Z. G. Shuai and Y. Zhao, *J. Chem. Phys.*, 2009, **130**, 024704.
7. Y. Geng, S. X. Wu, H. B. Li, X. D. Tang, Y. Wu, Z. M. Su and Y. Liao, *J. Mater. Chem.*, 2011, **21**, 15558-15566.
8. L. B. Schein and A. R. McGhie, *Phys. Rev. B*, 1979, **20**, 1631-1639.
9. W. J. Chi, Q. S. Li and Z. S. Li, *Nanoscale*, 2016, **8**, 6146-6154.
10. Z. Z. Sun and R. Long, *J. Phys. Chem. C*, 2023, **127**, 8953-8962.
11. Z. Z. Sun and R. Long, *J. Phys. Chem. C*, 2023, **127**, 12913-12922.

12. Z. Z. Sun, S. Feng, C. Gu, N. Cheng and J. Liu, *Phys. Chem. Chem. Phys.*, 2019, **21**, 15206-15214.
13. Z. Z. Sun, Y. L. Xu, R. Zhu and H. Y. Liu, *Org. Electron.*, 2018, **63**, 86-92.
14. J. Tomasi, B. Mennucci and R. Cammi, *Chem. Rev.*, 2005, **105**, 2999-3093.
15. T. Le Bahers, C. Adamo and I. Ciofini, *J. Chem. Theory Comput.*, 2011, **7**, 2498-2506.
16. T. Lu and F. W. Chen, *J. Comput. Chem.*, 2012, **33**, 580-592.
17. J. Ho, A. Klamt and M. L. Coote, *J. Phys. Chem. A*, 2010, **114**, 13442-13444.
18. M. J. Frisch, G. W. Trucks, H. B. Schlegel, *et al*., *Gaussian 09, Revision D.01*, Gaussian, Inc., Wallingford, CT, 2009.
19. B. Aradi, B. Hourahine and T. Frauenheim, *J. Phys. Chem. A*, 2007, **111**, 5678-5684.
20. J. Huang and M. Kertesz, *Chem. Phys. Lett.*, 2004, **390**, 110-115.
21. Z. Z. Sun, Y. Li and X. L. Xu, *Phys. Chem. Chem. Phys.*, 2024, **26**, 6817-6825.
22. T. Wang, Y. Li, Q. Cao, J. Yang, B. Yang, X. Pu, Y. Zhang, J. Zhao, Y. Zhang and H. Chen, *Energy Environ. Sci.* 2022, **15**, 4414-4424.
23. G. Kresse and J. Furthmuller, *Phys. Rev. B*, 1996, **54**, 11169-11186.
24. G. Kresse and J. Furthmuller, *Comput. Mater. Sci.*, 1996, **6**, 15-50.
25. J. P. Perdew, K. Burke and M. Ernzerhof, *Phys. Rev. Lett.*, 1996, **77**, 3865-3868.
26. P. E. Blochl, *Phys. Rev. B*, 1994, **50**, 17953-17979.
27. S. Grimme, *J. Comput. Chem.*, 2006, **27**, 1787-1799.

Table S1 Frontier molecular orbital energy levels of the investigated HTMs.

HTMs	E_{HOMO}				E_{LUMO}			
	B3LYP	B3LYP-R	PBE33	PBE38	B3LYP	B3LYP-R	PBE33	PBE38
SM-1	-4.69	-5.31	-5.27	-5.43	-2.35	-3.37	-2.13	-2.04
SM-2	-4.75	-5.38	-5.34	-5.50	-2.13	-3.10	-1.89	-1.78
SM-4	-4.83	-5.46	-5.42	-5.58	-2.30	-3.27	-2.06	-1.95

Table S2 Calculated ground- and excited-state properties of the designed HTMs with the CAM-B3LYP/6-31G** method.

HTMs	E_{H}[a]	E_{L}[b]	E_{H-L}[c]	λ_{abs}[d]	ΔE[e]	f[f]	$Assignment$[g]
SM-1	-5.91	-1.30	4.62	446	2.78	0.89	$H \rightarrow L$ (83%)
SM-2	-5.99	-1.02	4.97	367	3.38	1.49	$H \rightarrow L$(65%)
SM-4	-6.07	-1.19	4.87	370	3.35	1.83	$H \rightarrow L$(63%)

[a] Calculated HOMO energies (in eV). [b] Calculated LOMO energies (in eV). [c] Energy gaps (in eV). [d] Maximum absorption wavelengths (in nm). [e] Excitation energies (in eV). [f] Oscillator strengths. [g] Main orbital contributions (H = HOMO, L = LUMO).

Table S3 Calculated ground- and excited-state properties of the designed HTMs with the MPW1K/6-31G** method.

HTMs	E_{H}[a]	E_{L}[b]	E_{H-L}[c]	λ_{abs}[d]	ΔE[e]	f[f]	$Assignment$[g]
SM-1	-5.65	-1.93	3.72	481	2.58	0.78	$H \rightarrow L$ (92%)
SM-2	-5.73	-1.67	4.06	398	3.11	0.91	$H \rightarrow L$ (85%)
SM-4	-5.80	-1.84	3.96	405	3.06	1.11	$H \rightarrow L$ (85%)

[a] Calculated HOMO energies (in eV). [b] Calculated LOMO energies (in eV). [c] Energy gaps (in eV). [d] Maximum absorption wavelengths (in nm). [e] Excitation energies (in eV). [f] Oscillator strengths. [g] Main orbital contributions (H = HOMO, L = LUMO).

Table S4 Calculated ground- and excited-state properties of the designed HTMs with the wB97XD/6-31G** method.

HTMs	E_{H}[a]	E_{L}[b]	E_{H-L}[c]	λ_{abs}[d]	ΔE[e]	f[f]	$Assignment$[g]
SM-1	-6.51	-0.78	5.73	425	2.92	0.96	$H \rightarrow L$ (74%)
SM-2	-6.59	-0.51	6.08	350	3.54	1.90	$H \rightarrow L$ (50%)
SM-4	-6.66	-0.68	5.98	352	3.52	2.30	$H \rightarrow L$ (46%)

[a] Calculated HOMO energies (in eV). [b] Calculated LOMO energies (in eV). [c] Energy gaps (in eV). [d] Maximum absorption wavelengths (in nm). [e] Excitation energies (in eV). [f] Oscillator strengths. [g] Main orbital contributions (H = HOMO, L = LUMO).

Table S5 Calculated ground- and excited-state properties of the designed HTMs with the M06-2X/6-31G** method.

HTMs	E_{H}[a]	E_{L}[b]	E_{H-L}[c]	λ_{abs}[d]	ΔE[e]	f[f]	$Assignment$[g]
SM-1	-5.91	-1.63	4.28	447	2.77	0.94	$H \rightarrow L$ (88%)
SM-2	-5.99	-1.36	4.64	371	3.34	1.56	$H \rightarrow L$ (73%)
SM-4	-6.07	-1.53	4.53	378	3.28	1.80	$H \rightarrow L$ (71%)

[a] Calculated HOMO energies (in eV). [b] Calculated LOMO energies (in eV). [c] Energy gaps (in eV). [d] Maximum absorption wavelengths (in nm). [e] Excitation energies (in eV). [f] Oscillator strengths. [g] Main orbital contributions (H = HOMO, L = LUMO).

Table S6 Calculated charge transfer amounts (q_{ct}) and distances (d_{ct}) of the studied HTMs with the CAM-B3LYP/6-31G** and MPW1K/6-31G** methods.

HTMs	CAM-B3LYP		MPW1K	
	q_{ct}	d_{ct}	q_{ct}	d_{ct}
SM-1	0.77	1.30	0.84	1.31
SM-2	0.73	1.27	0.88	1.50
SM-4	0.77	1.11	0.92	1.52

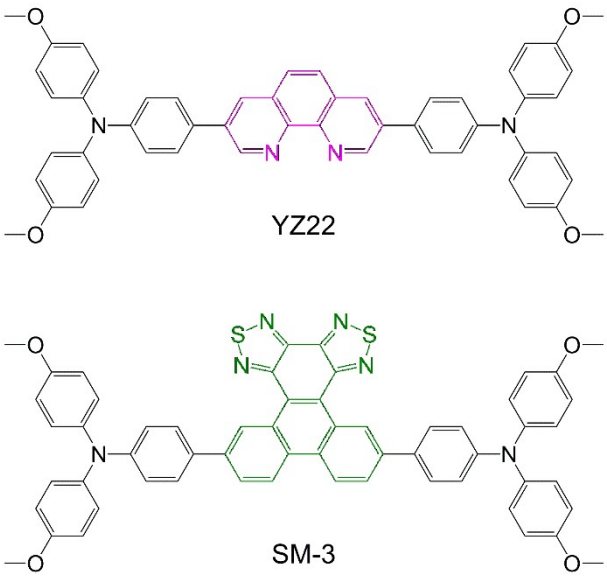

Fig. S1 Chemical structures of the YZ22 (*Energy Environ. Sci.*, 2020, **13**, 4334-4343) and SM-3 (*New J. Chem.*, 2020, **44**, 15244-15250).

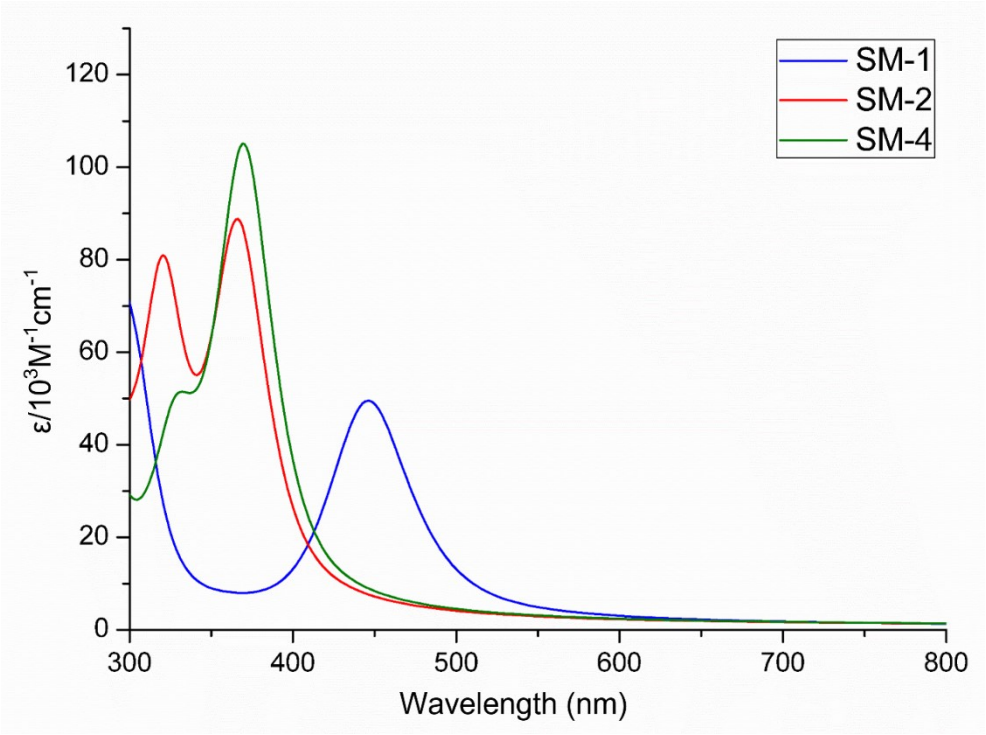

Fig. S2 Calculated vertical absorption light spectra of the investigated HTMs with the CAM-B3LYP/6-31G** method.

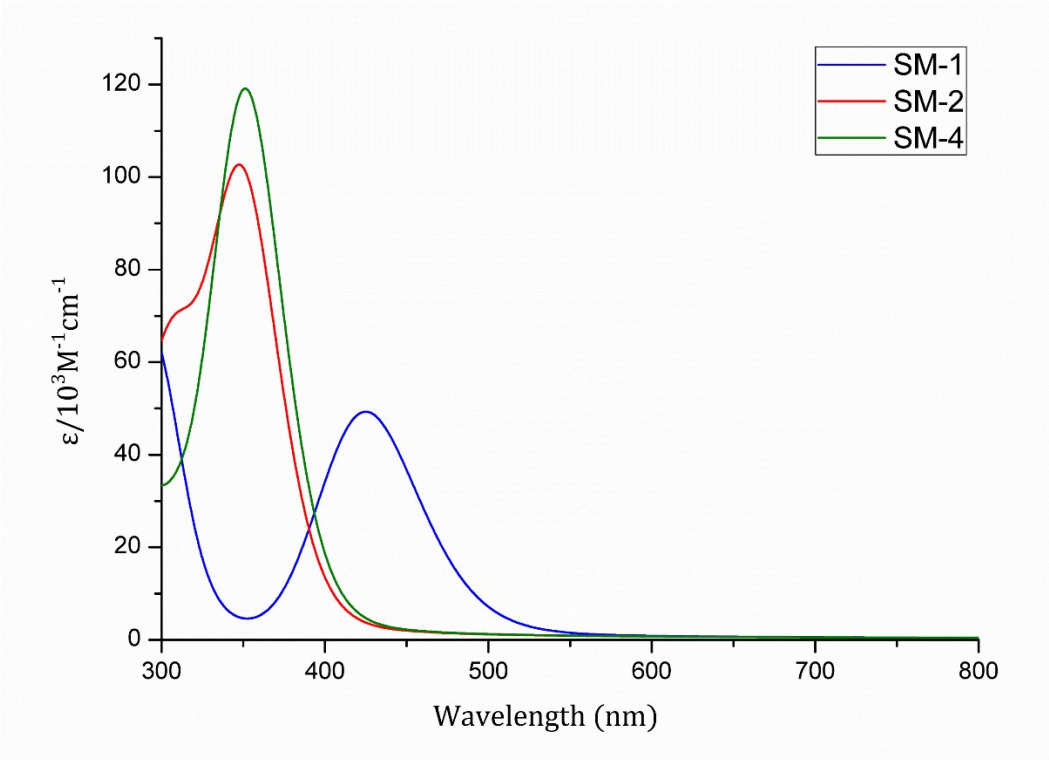

Fig. S3 Calculated vertical absorption light spectra of the investigated HTMs with the wB97XD/6-31G** method.

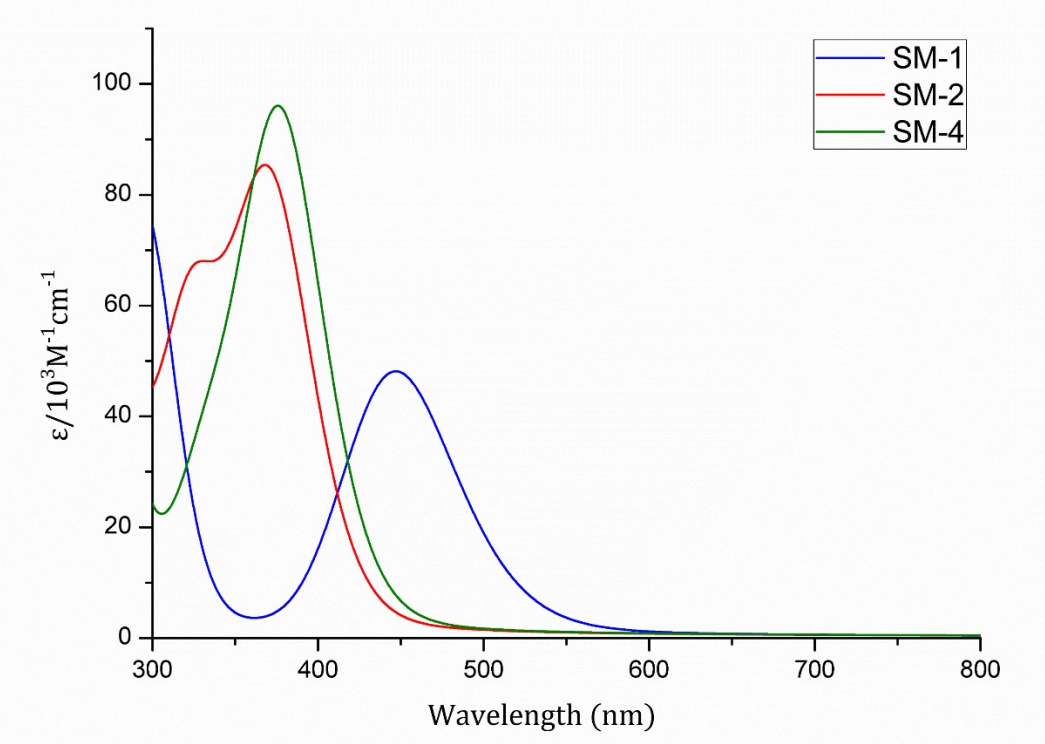

Fig. S4 Calculated vertical absorption light spectra of the investigated HTMs with the M06-2X/6-31G** method.

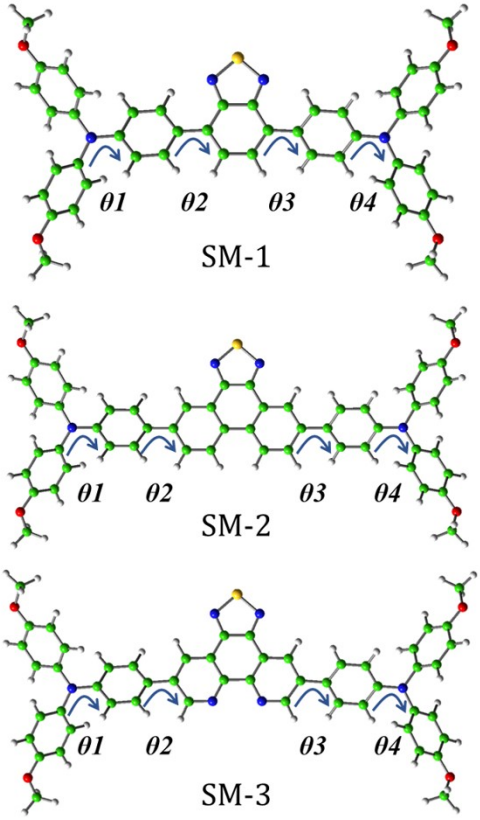

HTMs	Neutral state			
	θ1	*θ2*	*θ3*	*θ4*
SM-1	29.6	34	34	29.6
SM-2	30.5	31.7	31.7	30.6
SM-4	28.9	31.7	31.7	28.8
HTMs	Cationic state			
	θ1	*θ2*	*θ3*	*θ4*
SM-1	28.8	26.3	26.3	28.8
SM-2	36.6	30.6	30	29
SM-4	39.3	32.8	30.6	27.4
HTMs	Neutral-Cationic difference			
	θ1	*θ2*	*θ3*	*θ4*
SM-1	0.8	7.7	7.7	0.8
SM-2	6.1	1.1	1.7	1.6
SM-4	10.4	-1.1	1.1	1.4

Fig. S5 Optimized cationic geometries of investigated HTMs with selected dihedral angles, and the dihedral angle differences between neutral and cationic states.

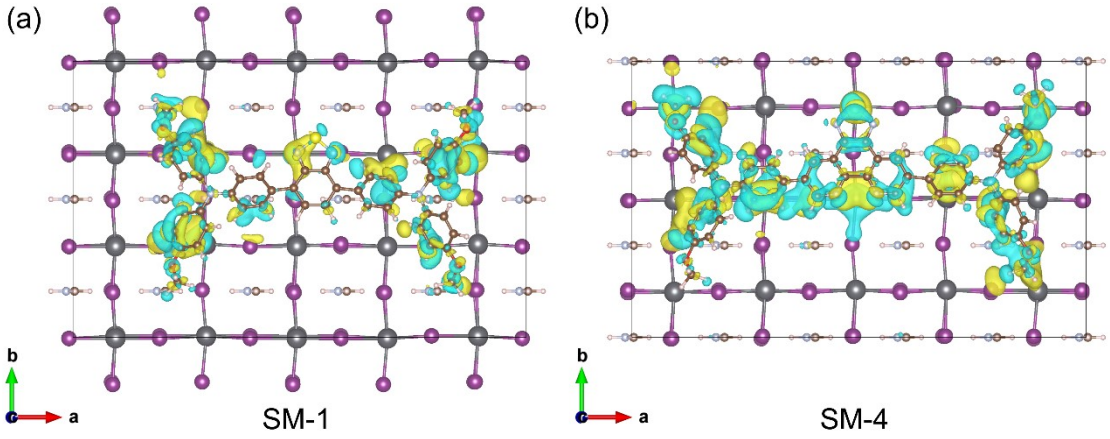

Fig. S6 Calculated charge density difference (CDD) maps of the adsorbed systems of $FAPbI_3$/SM-1 (a) and $FAPbI_3$/SM-4 (b) from the top view.

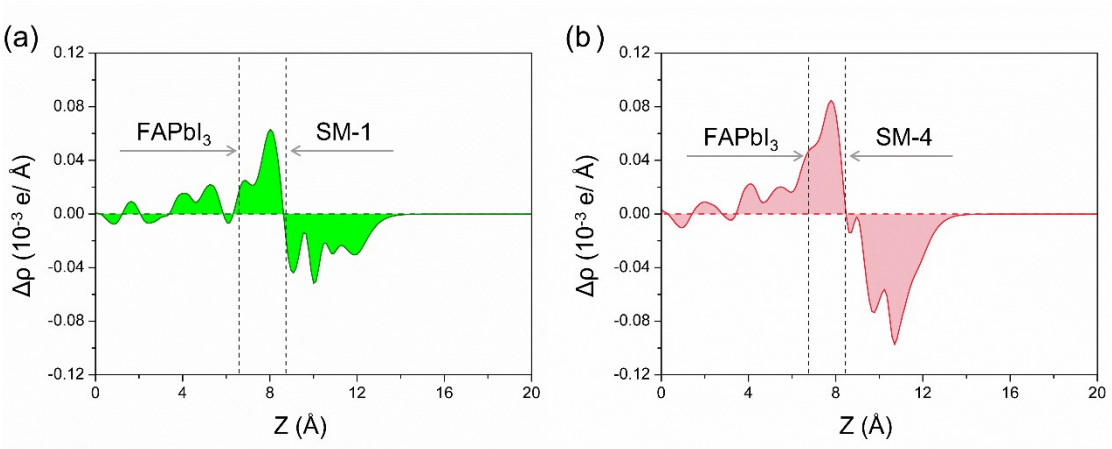

Fig. S7 Simulated planar-averaged CDD maps of $FAPbI_3$/SM-1 (a) and $FAPbI_3$/SM-4 (b) systems along z direction. The positive values mean the charge accumulation, and the negative values mean the charge depletion.